IEEE Photonics Journal
An IEEE Photonics Society Publication

Open Access

Photonic Wheels and Their Topological Reaction in a Strongly Focused Amplitude Tailored Beam

Volume 12, Number 2, April 2020

Wenrui Miao
Xiaoyan Pang, ***Member, IEEE***
Wenhao Liu

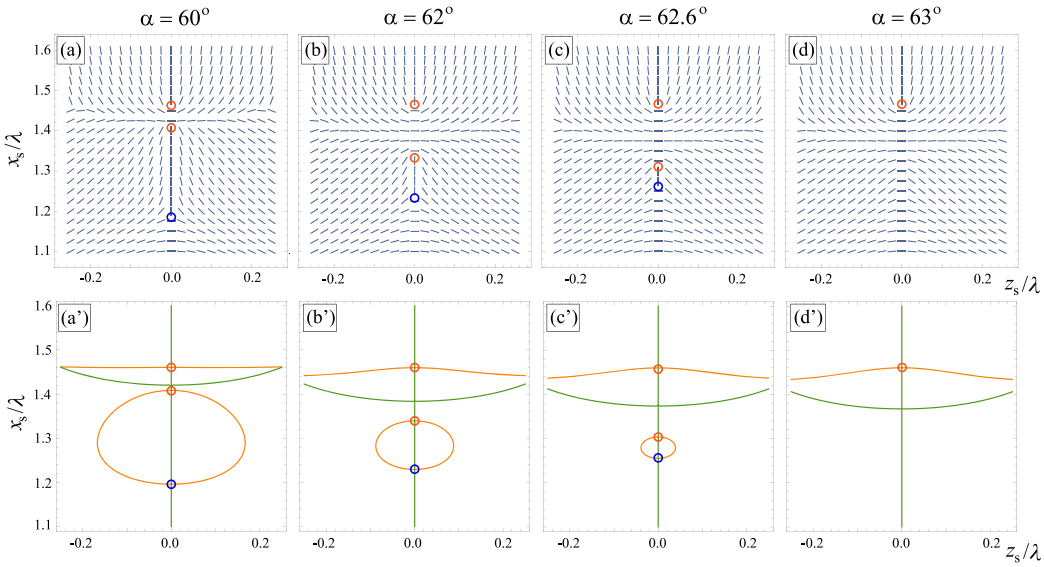

DOI: 10.1109/JPHOT.2020.2981347

Photonic Wheels and Their Topological Reaction in a Strongly Focused Amplitude Tailored Beam

Wenrui Miao,[1,2] **Xiaoyan Pang** ,[1] ***Member, IEEE*, and Wenhao Liu**[1]

[1]School of Electronics and Information, Northwestern Polytechnical University, Xi'an 710072, China
[2]Department of Physics and Optical Science, University of North Carolina at Charlotte, Charlotte, NC 28223 USA

DOI:10.1109/JPHOT.2020.2981347

Manuscript received January 19, 2020; revised March 11, 2020; accepted April 14, 2020. Date of publication March 17, 2020 This work was supported by National Natural Science Foundations of China under Grants 11974281 and 11504296. Corresponding author: Xiaoyan Pang (e-mail: xypang@nwpu.edu.cn).

Abstract: In this article, we propose a simple method to generate purely transverse spin density in a high numerical aperture system, and it is realized by focusing an amplitude tailored beam with a dipole-like shape. Through our analytical analysis, it is found that in this focused field the purely transverse spin density is not only confined in the focal plane, but also can exist in two mutually perpendicular meridional planes. Especially, the fields with purely transverse spin density are also examined from the view of topology. Two typical topological events which usually happen in traditional two dimensional transverse fields are observed in the meridional plane with purely transverse spin density, and it shows that the 'photonic wheels' follow the rule of topological index in their topological reactions. To the best of our knowledge, it is the first time to test the topological behavior of the field with purely transverse spin density. Our finding not only supplies a simple way to generate 'photonic wheels' in three planes of the field, but also adds new features to the field containing 'photonic wheels'.

Index Terms: Transverse spin density, polarization, topological reaction, photonic wheel.

1. Introduction

Light can possess both spin and orbital angular momenta (SAM and OAM) which are associated with circular polarization and optical vortex, respectively. SAM and OAM play crucial roles in both fundamental researches [1]–[3] and applied areas, for instance in laser cooling [4], in optical manipulation [5] and communications [6], [7]. The SAM density (also called spin density for brevity), in a classical two dimensional (2D) optical field is always taken as a scalar because it only has a longitudinal component parallel with the propagation direction. However, in light fields within nonparaxial regime, like strongly focused fields or near field, the longitudinal component of the field cannot be negligible, i.e. the field is three dimensional (3D). In such 3D fields, the transverse component of the spin density exists and the orientation of the 'spin density vector' can be arbitrary in 3D space [8]–[10], leading to interesting structures of 3D fields, such as spiral spin density vectors [11]–[13], polarization Möbius strip [14]–[16] and topological knots [17], [18]. It has been demonstrated that the transverse spin density has a strong connection with

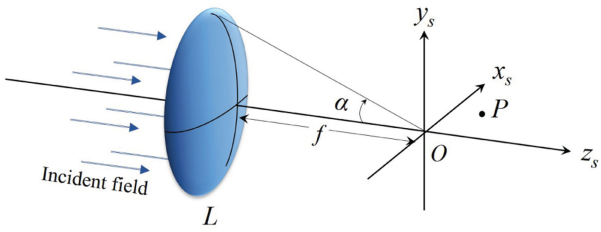

Fig. 1. Illustration of a high-numerical-aperture system. The propagation axis is z_s.

geometrical spin Hall effect of light [19]–[22] and is quite useful in nano-optics, like in observation of spin-orbit interaction [23], controlling the light-matter interaction [24] and the emission directivity of a dipole-like nanoparticle [25]. Particularly, if the spin density is purely transverse, i.e. the longitudinal component of the spin density is zero, the electric field vector will spin in the propagation plane (containing the propagation axis), thus a 'photonic wheel' occurs [26]–[30]. Fields containing 'photonic wheels' are perfect candidates for investigating the properties of the transverse spin density, and in most researches such fields are usually generated in a high numerical aperture (NA) system by focusing the beam with very complicated form, for instance the polarization tailored beams, like the beam with two spatially separated left- and right-handed circular polarization [26], the radially polarized beam [29] and full poincaré beams [31], also the amplitude-phase-polarization jointly tailored beam [32]. In this article, we will show that just by tailoring the amplitude of the incident beam, the purely transverse spin density also can be generated in the focal region.

On the other hand, when the field is studied in topology, the optical singularities and the topological structures around them are main concerns [33]–[35]. The circular polarization in singular optics corresponds to a kind of polarization singularity, i.e. a C point. In the electromagnetic fields, the C point and its topological behaviors feature the topological characteristics of the fields and have been studied in a variety of fields from the random field to the deterministic field [33], [35]–[37] where many interesting phenomena are observed, like polarization Möbius strip [14]–[16] and topological polarization knots [18], Berry's paradox for polarization singularities [38], [39]. In recent times, there are still a lot attention paid on the generation of structured fields with various polarization singularities and observation of topological reactions there [40]–[44]. Since the SAM and the spin density have a close relation with the C points, and purely transverse spin density actually reflects the field with polarization ellipses lying in 2D meridional planes, it will be very interesting to examine these 'photonic wheels' in the view of topology. Although the topological laws should be valid for any topological event in both 2D transverse fields (under paraxial approximation) and 3D fields (without paraxial approximation), no topological behavior has been tested or observed for the polarization ellipses lying in the plane containing the propagation direction. Therefore in this article, we will also examine the topological reactions in the field with purely transverse spin density, and as it will be shown that the two typical topological events occur for the 'photonic wheels'.

2. Focused Field

First consider an aplanatic high NA system with a semi-aperture angle α and a focal length f (see Fig. 1). Then we assume that incident field is an amplitude tailored Gaussian beam whose complex amplitude at the entrance plane can be expressed as

$$V_0(\rho, \phi) = \rho e^{-\rho^2/w_0^2} \cos\phi, \tag{1}$$

where $\rho = \sqrt{x^2 + y^2}$ is the radial distance and ϕ is the azimuthal angle. The intensity and the phase distribution of the incident field are shown in Fig. 2, and we can see that this beam bears a shape similar to a dipole, having two lobes located symmetrically with respect to the y axis and the phases at two half planes (for $-x$ and $+x$ half planes) having a π shift. The white line along the y axis in

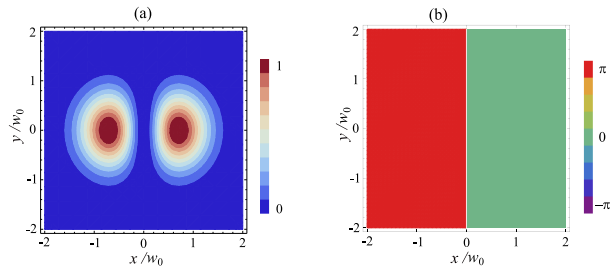

Fig. 2. Intensity (a) and phase (b) distribution of the incident wave at the entrance plane.

Fig. 2(b) indicates the phase singularities for the zero intensity there. Strictly speaking, this beam may be said to be both amplitude and phase tailored, which can be generated by a spacial light modulator (SLM) or can be treated as a superposition of two vortex beams with opposite topological charges (i.e. topological charge $t = +1$ and $t = -1$ for each beam).[1]

Now suppose that this amplitude tailored, dipole-shaped beam has uniform polarization and its electric field is oscillating along the x direction (i.e. x polarized). According to the Richards&Wolf vectorial diffraction theory [45], the electric field components of this strongly focused, linearly polarized field at observation point $P(x_s, y_s, z_s)$ in the focal region can be calculated and written as follows:

$$e_x(\rho_s, z_s, \phi_s) = \frac{k}{4}\int_0^{\alpha} f^2 \sin^2\theta \sqrt{\cos\theta}\, e^{-f^2\sin^2\theta/w_0^2} \left(I_{x1}\left[\theta, \rho_s, \phi_s\right) + I_{x3}(\theta, \rho_s, \phi_s)\right] e^{ikz_s\cos\theta} d\theta, \tag{2}$$

$$e_y(\rho_s, z_s, \phi_s) = \frac{k}{4}\int_0^{\alpha} f^2 \sin^2\theta \sqrt{\cos\theta}\, e^{-f^2\sin^2\theta/w_0^2} \left[I_{y1}(\theta, \rho_s, \phi_s) + I_{y3}(\theta, \rho_s, \phi_s)\right] e^{ikz_s\cos\theta} d\theta, \tag{3}$$

$$e_z(\rho_s, z_s, \phi_s) = -\frac{ik}{2}\int_0^{\alpha} f^2 \sin^2\theta \sqrt{\cos\theta}\, e^{-f^2\sin^2\theta/w_0^2} \left[I_{z0}(\theta, \rho_s, \phi_s) + I_{z2}(\theta, \rho_s, \phi_s)\right] e^{ikz_s\cos\theta} d\theta, \tag{4}$$

and

$$I_{x1}(\theta, \rho_s, \phi_s) = \cos\phi_s(3\cos\theta + 1)J_1(k\rho_s\sin\theta), \tag{5}$$

$$I_{x3}(\theta, \rho_s, \phi_s) = \cos 3\phi_s(1 - \cos\theta)J_3(k\rho_s\sin\theta), \tag{6}$$

$$I_{y1}(\theta, \rho_s, \phi_s) = -\sin\phi_s(1 - \cos\theta)J_1(k\rho_s\sin\theta), \tag{7}$$

$$I_{y3}(\theta, \rho_s, \phi_s) = \sin 3\phi_s(1 - \cos\theta)J_3(k\rho_s\sin\theta), \tag{8}$$

$$I_{z0}(\theta, \rho_s, \phi_s) = -\sin\theta J_0(k\rho_s\sin\theta), \tag{9}$$

$$I_{z2}(\theta, \rho_s, \phi_s) = \cos 2\phi_s \sin\theta J_2(k\rho_s\sin\theta), \tag{10}$$

where J_n is the first kind of Bessel function of nth order and $\rho_s = \sqrt{x_s^2 + y_s^2}$. The subscript of e_j ($j = x, y, z$) represents the j-polarized field component. In the following all the analyses are based on the expression of the focused field, Eqs. (2)–(10). It is worth noting that when the input field is not x polarized, for instance y polarized or circular polarized, the focused field will be quite different and the results presented in this article will no longer be observed. It is quite clear that the focused field has three field components, so that the polarization ellipse at any point in this 3D field is not confined in the transverse plane (i.e., x_s-y_s plane), but can lie in any plane in 3D space. The spin density vector of electric field, $\mathbf{s}_E$ is also a quantity describing the 3D polarization state with the

[1]It was reminded by a reviewer that the incident beam very resembled the classical Hermite-Gauss beam, the HG10 mode. Then we found that the expression of the HG10 beam at its beam waist can be written in the form of Eq. (1). Thus the general behaviors of the 'photonic wheels' discussed here will also be valid for the incident HG10 beam, but since the topological structures are very sensitive to the field change, the topological behaviors presented in this article may have difference from those in a strongly focused HG10 beam.

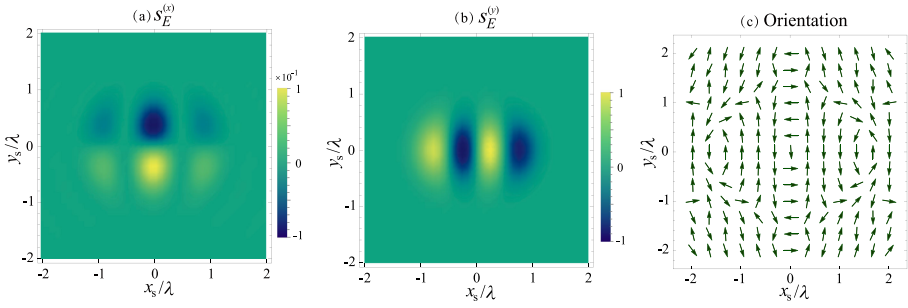

Fig. 3. Spin density distribution at the focal plane. (a) $s_E^{(x)}$, (b) $s_E^{(y)}$ and (c) the orientation of the spin density vectors. Here $\alpha = 60^\circ$, $f/w_0 = 2$.

absolute value of $\mathbf{s}_E$ reflecting the shape of the polarization ellipse and the direction of the vector indicating the orientation of the polarization plane. The definition of the spin density vectors of the electric field can be expressed as [2], [29], [36] as

$$\mathbf{s}_E = \begin{pmatrix} s_E^{(x)} \\ s_E^{(y)} \\ s_E^{(z)} \end{pmatrix} = \frac{\epsilon_0}{2\omega} \begin{pmatrix} |e_y||e_z| \sin\phi_{zy} \\ |e_x||e_z| \sin\phi_{zx} \\ |e_x||e_y| \sin\phi_{yx} \end{pmatrix}, \tag{11}$$

where $\phi_{ij} = \phi_i - \phi_j$ $(i, j = x, y, z)$ is the phase difference between two field components e_i and e_j. In the following part, we will see that in this focused field the spin density vectors have very striking behaviors: in three mutually perpendicular planes, the spin density vectors are all purely transverse.

3. Purely Transverse Spin Density

Let's first examine the field at the focal plane. When $z_s = 0$, it is not hard to find that the e_x and e_y components are in phase or out of phase, indicating that the z component of the spin density vector, $s_E^{(z)}$ is zero [see Eq. (11)], i.e., no longitudinal component of the spin density vectors in the focal plane. Furthermore, the imaginary factor in the e_z component causes a $\pi/2$ phase difference between the longitudinal and transverse field components, so that the transverse components $s_E^{(x)} = \pm(\epsilon_0/2\omega)|e_y||e_z|$ and $s_E^{(y)} = \pm(\epsilon_0/2\omega)|e_x||e_z|$. Therefore, we can say that the spin density vectors are purely transverse in the focal plane. In another word, here the electric field vectors spin in the planes perpendicular to the focal plane, i.e., the 'photonic wheels' are formed. As an example, the transverse spin density components $s_E^{(x)}$ and $s_E^{(y)}$, and the orientation of the spin density vectors in the focal plane are illustrated in Fig. 3, where the Green arrow denotes the orientation of the local spin density vector. Here the spin densities in Figs. 3(a) and (b) are both normalized to the maximum value of $|s_E^{(y)}|$. We can see that the $s_E^{(x)}$ and $s_E^{(y)}$ have different distributions and the spin density vectors can have arbitrary transverse orientations in the focal plane.

The orientation and the distribution of the spin density vectors can be controlled by the semi-aperture angle α. In Fig. 4 the orientation of the spin density vectors are shown for $\alpha = 45^\circ$ and 30°. Comparing the Fig. 4 with Fig. 3(c), we can see that as α decreases, there are more spin density vectors orienting towards y_s axis. Since the maxima of the $|s_E^{(x)}|$ (or $|s_E^{(y)}|$) lie on the y_s axis (or the x_s axis) [see Figs. 3(a) and (b)], it is convenient to focus on the $s_E^{(x)}$ and $s_E^{(y)}$ only on the y_s axis and the x_s axis separately to examine their variations with α, and this is shown in Fig. 5 where the $s_E^{(x)}$ and $s_E^{(y)}$ are normalized to the maximum value of $|s_E^{(y)}|$. As the semi-aperture angle α decreases, both the $|s_E^{(x)}|$ and $|s_E^{(y)}|$ decrease significantly, especially for the $s_E^{(x)}$ component. This is because that $s_E^{(x)} \propto |e_y||e_z|$, $s_E^{(y)} \propto |e_x||e_z|$ where both the e_y and e_z components, the consequence of the strongly focusing, will be reduced greatly with decreasing the semi-aperture angle α, while the

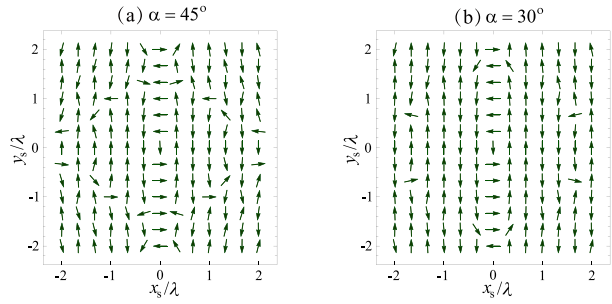

Fig. 4. The orientation of the spin density vectors for different semi-aperture angle α. (a) $\alpha = 45^\circ$, (b) $\alpha = 30^\circ$.

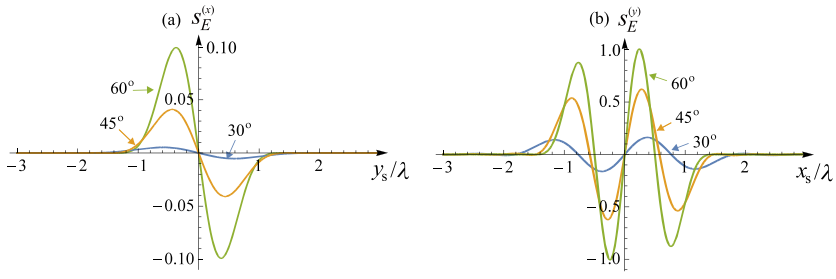

Fig. 5. Variation of the spin density on the y_s axis (a) and the x_s axis (b) with semi-aperture angle α.

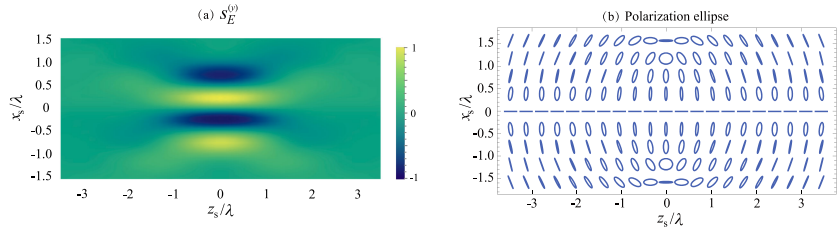

Fig. 6. Spin density distribution on the x_s-z_s plane. (a) $s_E^{(y)}$, (b) polarization ellipses. Here $\alpha = 60^\circ$, $f/w_0 = 2$.

$|e_x|$ component will not be influenced strongly by α. That is also the reason why in Fig. 4(b) there are more y_s-oriented vectors.

Second, by observing the expressions of the focused field [Eqs. (2)-(10)], we can find that when $\phi_s = 0$ or π, $l_{y1} = l_{y3} = 0$ so that $e_y = 0$, which leads to $s_E^{(x)} = s_E^{(z)} = 0$. Thus in the x_s-z_s plane, only the y component of the spin density vector $s_E^{(y)}$ exists, i.e. the purely transverse spin density. It also means that here the electric field vectors spin around the y_s axis transverse to the beam's propagation direction. The spin density distribution and the corresponding local polarization ellipses in the x_s-z_s plane are shown in Fig. 6. It is clear to see that all the polarization ellipses lie in the plane (the x_s-z_s plane) parallel to the propagation direction. Similarly, at the plane with $\phi_s = \pi/2$ or $3\pi/2$, $l_{x1} = l_{x3} = 0$ thus $e_x = 0$, which leads to $s_E^{(y)} = s_E^{(z)} = 0$. So in the y_s-z_s plane, there only exists the x component of the spin density vector $s_E^{(x)}$, i.e. the purely transverse spin density. As it happened in the x_s-z_s plane, the electric vectors in the y_s-z_s plane also spin around the x_s axis transverse to the propagation axis and the polarization ellipses there lie in the plane (the y_s-z_s plane), which can be seen in Fig. 7. Here we should note that firstly the spin density vectors in these two mutually perpendicular meridional planes are also perpendicular to each other, secondly as it happens in

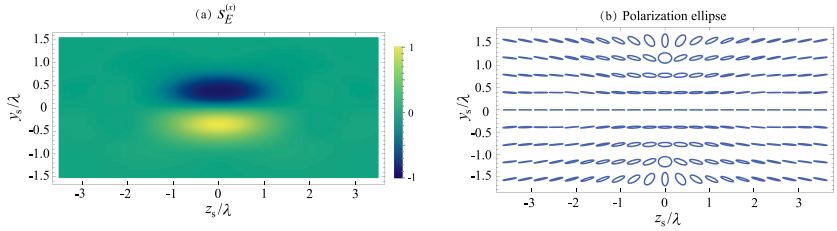

Fig. 7. Spin density distribution on the y_s-z_s plane. (a) $s_E^{(e)}$, (b) polarization ellipses. Here $\alpha = 60^\circ$, $f/w_0 = 2$.

the focal plane, the spin density in the x_s-z_s and y_s-z_s planes also can be enhanced in general by increasing the semi-aperture angle α.

Therefore, in this focused amplitude tailored field, the purely transverse spin density are generated not only in the focal plane but also in the other two mutually perpendicular meridional planes (the x_s-z_s plane and the y_s-z_s plane). The purely transverse spin density in these three planes all can be increased by enlarging the semi-aperture angle α. Furthermore, we can find from Figs. 6(b) and 7(b) that the polarization can be in any state in the x_s-z_s or y_s-z_s planes, i.e., the circular polarization corresponding to a type of polarization singularity (i.e. a C-point) also can be observed. So in the following section, we will examine the field with purely transverse spin density from the view of topology and show that these 'photonic wheels' also can have topological reactions.

4. Topological Reactions of the 'Photonic Wheel'

The topological reactions usually describe the behaviors of the topological structures around optical singularities in traditionally 2D transverse fields, for instance in the x-y planes for the beam propagating along the z axis. A C-point, as a type of polarization singularities, plays a main role in the topological reactions of 2D electromagnetic fields. As we analyzed in previous section, in the x_s-z_s plane or the y_s-z_s plane the polarization ellipses lie in these planes, which is analogous to the traditional polarization ellipses in the transverse planes of 2D optical fields. Therefore by using the same way of analysis in traditional transverse fields, we can study the topological structures of these polarization ellipses in these two meridional planes, i.e., the topological behavior of the field with purely transverse spin density. First, we recall the Stokes parameters, S_0, S_1, S_2 and S_3 used in 2D transverse fields, but adapt them based on current field, as

$$S_0 = |e_i|^2 + |e_z|^2, \tag{12}$$

$$S_1 = |e_i|^2 - |e_z|^2, \tag{13}$$

$$S_2 = 2|e_i||e_z|\cos\phi_{iz}, \tag{14}$$

$$S_3 = 2|e_i||e_z|\sin\phi_{iz}, \tag{15}$$

where $\phi_{iz} = \arg[e_i] - \arg[e_z]$, $(i = x, y)$ is still the phase difference between two fields e_i and e_z. The normalized Stokes parameters are $s_1 = S_1/S_0$, $s_2 = S_2/S_0$ and $s_3 = S_3/S_0$ which also represents a point on the Poincaré sphere [46, Sec. 1.4][47, Sec. 10.3]. A C-point occurs at the position where the $|s_3| = 1$ (or $s_1 = s_2 = 0$). C points possess a conserved topological index [33], [34], which can be defined as the number of rotations that the polarization ellipse undergoes as one travels a closed path around a polarization singularity, and it can be expressed mathematically as [35]:

$$n = \frac{1}{2\pi}\oint_L \nabla\psi(\mathbf{r})\cdot d\mathbf{r}, \tag{16}$$

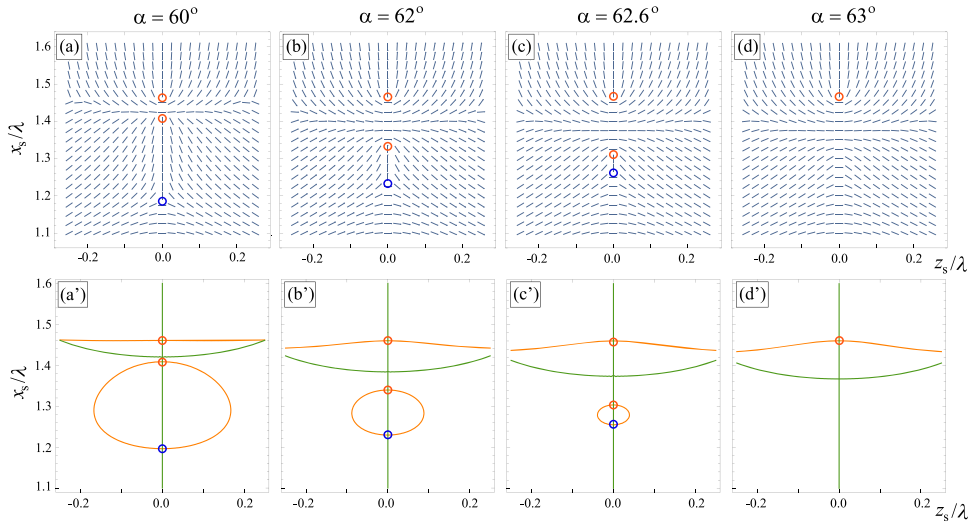

Fig. 8. Annihilation/creation event on the x_s-z_s plane. (a)–(d) The local orientation of the major axis of the polarization ellipse. (a')–(d') Selected contours of the normalized Stokes parameters for the same region as in the upper panel: $s_1 = 0$ (orange), $s_2 = 0$ (green).

where $\psi(\mathbf{r})$ represents the orientation angle of the polarization ellipse and L is a closed path of integration around the polarization singularity. There are three generic patterns of the polarization ellipses in the vicinity of a C point: a lemon ($n = +1/2$), a star ($n = -1/2$) and a monstar ($n = -1/2$) [33]–[35]. The monstar is actually a transition structure which only appears just before creation/annihilation events.

Now we put $i = x$ in Eqs. (12)–(15) and focus on the topological reactions in the x_s-z_s plane. Fig. 8 shows an annihilation/creation event of the topological structures around C-points on the x_s-z_s plane. The short line of dark blue in Fig. 8(a)–(d) represents the local orientation of the major axis of the polarization ellipse. The red circle and blue circle denote the C-points with $n = +1/2$ and $n = -1/2$, respectively. In Fig. 8(a')–(d') the orange curve is the contour line of normalized stokes parameter $s_1 = 0$, while the green curve is the contour line of $s_2 = 0$, so that the intersection of these two curves indicates a C-point ($s_1 = 0$, $s_2 = 0$ and $|s_3| = 1$). When $\alpha = 60^\circ$, in Fig. 8(a) we can find three C-points near (0,1.46), (0,1.41) and (0,1.19) corresponding to three topological patterns: a lemon ($n = +1/2$), a lemon ($n = +1/2$) and a star ($n = -1/2$) respectively. As α increases from 60°, 62° to 62.6°, the lower lemon and the star move closer and closer [see Fig. 8(b) and (c) or (b') and (c')], and at the semi-aperture angle $\alpha = 63^\circ$ [Fig. 8(d) or (d')] that lemon and the star annihilate with each other. If it is seen from Fig. 8(d) to (a) [or (d') to (a')], the creation process is observed. In this annihilation/creation event, the topological index is conserved, i.e., the total value of the index in this observation region is always $+1/2 + 1/2 - 1/2 = +1/2$, indicating no single C-point appeared or disappeared.

On another way, if the semi-aperture angle α is decreased from 60° to 58°, another topological even will occur. This is shown in Fig. 9, where we can see that as α decreases, rather than the interaction of one lemon and one star, the two adjacent lemons begin to merge, resulting in a second-order polarization singularity: a node ($n = +1$). In Fig. 9(c) and (c') the node is marked by two red concentric circles, and we also can see that the node is the intersection of two orange curves ($s_1 = 0$) and two green curves ($s_2 = 0$) in Fig. 9(c'). Note that in Fig. 9(b) and (c) or (b') and (c') there also appear another two C-points located near ($\pm 0.2, 1.48$) which will not be discussed further in this article. Additionally by using the same method the topological reactions in the y_s-z_s plane also can be observed.

In summary, in this section by using an adapted Stokes parameters, two typical topological events are observed in the x_s-z_s plane where the spin density vectors of the field are purely transverse.

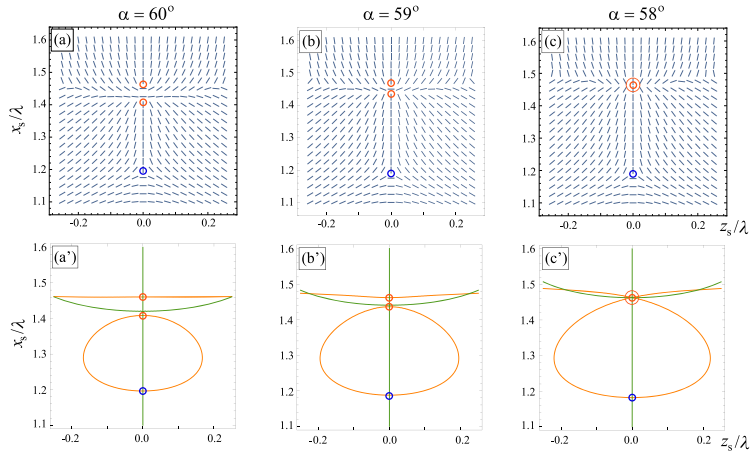

Fig. 9. Formation of a node on the x_s-z_s plane. (a)–(c) The local orientation of the major axis of the polarization ellipse. (a')–(c') Selected contours of the normalized Stokes parameters for the same region as in the upper panel: $s_1 = 0$ (orange), $s_2 = 0$ (green).

The observation shows that the topological reactions of these 'photonic wheels' also obey the conservation law of the topological index.

5. Conclusion

In this article, an amplitude tailored beam is proposed for generation of purely transverse spin density in a strongly focusing system. It has been demonstrated that in the focused field the purely transverse spin density, or the 'photonic wheel' not only exists in the focal plane, but also can be found in the other two planes perpendicular to the focal plane, i.e. the meridional planes. The transverse spin density in all these three mutually perpendicular planes can be enhanced by increasing the semi-aperture angle α. Especially, through adapting the traditional 2D Stokes parameters, to the best of our knowledge, it is the first time of observation of topological reaction for the 'photonic wheels' in the plane containing the propagation direction. It has been shown that the topological behaviors of the field with purely transverse spin density also obey the conservation law of the topological index. The 'photonic wheels' in three planes can be tested by the nanoprobe scanning measurement [8], and the topological structures may be observed experimentally through the 3D nanotomography of optical vector field adopted in [16], [18]. Our finding in this article not only provides a new candidate for investigating the transverse spin density, but also supports a new way, from the topological perspective, to study the 'photonic wheel'.

References

[1] L. Allen, S. M. Barnett, and M. J. Padgett, *Optical Angular Momentum*. Bristol, U.K.: IoP Publishing, 2003.
[2] K. Y. Bliokh, A. Y. Bekshaev, and F. Nori, "Extraordinary momentum and spin in evanescent waves," *Nat. Commun.*, vol. 5, no. 3, 2014, Art. no. 3300.
[3] K. Y. Bliokh, F. J. Rodríguezfortuño, F. Nori, and A. V. Zayats, "Spin-orbit interactions of light," *Nature Photon.*, vol. 9, no. 12, pp. 156–163, 2015.
[4] S. Stenholm, "The semiclassical theory of laser cooling," *Rev. Mod. Phys.*, vol. 58, no. 3, pp. 699–739, 1986.
[5] K. Dholakia and T. Čižmár, "Shaping the future of manipulation," *Nature Photon.*, vol. 5, no. 6, pp. 335–342, 2011.
[6] J. Wang *et al.*, "Terabit free-space data transmission employing orbital angular momentum multiplexing," *Nature Photon.*, vol. 6, pp. 488–496, 2012.
[7] P. Gregg, P. Kristensen, A. Rubano, S. Golowich, L. Marrucci, and S. Ramachandran, "Enhanced spin orbit interaction of light in highly confining optical fibers for mode division multiplexing," *Nat. Commun.*, vol. 10, 2019, Art. no. 4707.
[8] M. Neugebauer, T. Bauer, A. Aiello, and P. Banzer, "Measuring the transverse spin density of light," *Phys. Rev. Lett.*, vol. 114, no. 6, 2015, Art. no. 063901.

[9] A. Y. Bekshaev, K. Y. Bliokh, and F. Nori, "Transverse spin and momentum in two-wave interference," *Phys. Rev. X*, vol. 5, no. 1, 2015, Art. no. 011039.
[10] S. Saha, A. K. Singh, S. K. Ray, A. Banerjee, S. D. Gupta, and N. Ghosh, "Transverse spin and transverse momentum in scattering of plane waves," *Opt. Lett.*, vol. 41, no. 19, pp. 4499–4502, 2016.
[11] X. Pang and W. Miao, "Spinning spin density vectors along the propagation direction," *Opt. Lett.*, vol. 43, no. 19, pp. 4831–4834, 2018.
[12] J. Zhuang, L. Zhang, and D. Deng, "Tight-focusing properties of linearly polarized circular Airy Gaussian vortex beam," *Opt. Lett.*, vol. 45, no. 2, pp. 296–299, 2020.
[13] X. Pang, W. Liu, and W. Miao, "Generation of spiral spin density vectors with a circularly polarized, vortex beam," *IEEE Photonics J.*, to be published, doi: 10.1109/JPHOT.2019.2961148.
[14] I. Freund, "Cones, spirals, and möbius strips, in elliptically polarized light," *Opt. Commun.*, vol. 249, no. 1-3, pp. 7–22, 2005.
[15] I. Freund, "Optical möbius strips and twisted ribbon cloaks," *Opt. Lett.*, vol. 39, no. 4, pp. 727–730, 2014.
[16] T. Bauer *et al.*, "Observation of optical polarization möbius strips," *Science*, vol. 347, no. 6225, pp. 964–966, 2015.
[17] M. R. Dennis, R. P. King, B. Jack, K. OHolleran, and M. J. Padgett, "Isolated optical vortex knots," *Nature Phys.*, vol. 6, no. 2, pp. 118–121, 2010.
[18] H. Larocque *et al.*, "Reconstructing the topology of optical polarization knots," *Nature Phys.*, vol. 14, no. 11, pp. 1079–1082, 2018.
[19] A. Aiello, N. Lindlein, C. Marquardt, and G. Leuchs, "Transverse angular momentum and geometric spin hall effect of light," *Phys. Rev. Lett.*, vol. 103, no. 10, 2009, Art. no. 100401.
[20] M. Neugebauer *et al.*, "Geometric spin hall effect of light in tightly focused polarization-tailored light beams," *Phys. Rev. A*, vol. 89, no. 1, 2014, Art. no. 013840.
[21] J. Korger *et al.*, "Observation of the geometric spin Hall effect of light," *Phys. Rev. Lett.*, vol. 112, no. 11, 2014, Art. no. 113902.
[22] X. Ling *et al.*, "Recent advances in the spin hall effect of light," *Rep. Prog. Phys.*, vol. 80, no. 6, 2017, Art. no. 066401.
[23] Z. Shao, J. Zhu, Y. Chen, Y. Zhang, and S. Yu, "Spin-orbit interaction of light induced by transverse spin angular momentum engineering," *Nat. Commun.*, vol. 9, 2018, Art. no. 926.
[24] C. Junge, D. OShea, J. Volz, and A. Rauschenbeutel, "Strong coupling between single atoms and nontransversal photons," *Phys. Rev. Lett.*, vol. 110, no. 21, 2013, Art. no. 213604.
[25] M. Neugebauer, T. Bauer, P. Banzer, and G. Leuchs, "Polarization tailored light driven directional optical nanobeacon," *Nano Lett.*, vol. 14, no. 5, pp. 2546–2551, 2014.
[26] P. Banzer *et al.*, "The photonic wheel - demonstration of a state of light with purely transverse angular momentum," *J. Europ. Opt. Soc. Rap. Public.*, vol. 8, 2013, Art. no. 13032.
[27] K. Y. Kim, "Transverse spin angular momentum of airy beams," *IEEE Photon. J.*, vol. 4, no. 6, pp. 2333–2339, Dec. 2012.
[28] A. Aiello, P. Banzer, M. Neugebauer, and G. Leuchs, "From transverse angular momentum to photonic wheels," *Nature Photon.*, vol. 9, no. 12, pp. 789–795, 2015.
[29] T. Bauer, M. Neugebauer, G. Leuchs, and P. Banzer, "Optical polarization möbius strips and points of purely transverse spin density," *Phys. Rev. Lett.*, vol. 117, no. 1, 2016, Art. no. 013601.
[30] A. Aiello and P. Banzer, "The ubiquitous photonic wheel," *J. Optics*, vol. 18, no. 8, 2016, Art. no. 085605.
[31] W. Zhu, V. Shvedov, W. She, and W. Krolikowski, "Transverse spin angular momentum of tightly focused full poincaré beams," *Opt. Express*, vol. 23, no. 26, 2015, Art. no. 34029.
[32] C. Jian, W. Chenhao, K. Lingjiang, and Q. Zhan, "Experimental generation of complex optical fields for diffraction limited optical focus with purely transverse spin angular momentum," *Opt. Express*, vol. 25, no. 8, pp. 8966–8974, Apr. 2017.
[33] J. F. Nye, *Natural Focusing and Fine Structure of Light*. London, U.K.: Institute of Physics, 1999.
[34] M. R. Dennis, K. O'Holleran, and M. J. Padgett, "Singular optics: Optical vortices and polarization singularities," in *Progress in Optics*, E. Wolf, Ed. Amsterdam, The Netherlands: Elsevier, 2009, vol. 53, pp. 293–363.
[35] G. J. Gbur, *Singular Optics*. Boca Raton, FL, USA: CRC Press, 2017.
[36] M. V. Berry and M. R. Dennis, "Polarization singularities in isotropic random vector waves," *Proc. R. Soc. A*, vol. 457, no. 2005, pp. 141–155, 2001.
[37] M. V. Berry, "Index formulae for singular lines of polarization," *J. Opt. A*, vol. 6, no. 6, 2004, Art. no. 675.
[38] M. V. Berry, "Circular lines of circular polarization in three dimensions, and their transverse-field counterparts," *J. Opt.*, vol. 15, no. 4, 2013, Art. no. 044024.
[39] I. Freund, "Observer-dependent sign inversions of polarization singularities," *Opt. Lett.*, vol. 39, no. 20, pp. 5873–5876, Oct. 2014.
[40] X. Pang, G. Gbur, and T. D. Visser, "Cycle of phase, coherence and polarization singularities in Youngs three-pinhole experiment," *Opt. Express*, vol. 23, no. 26, pp. 34 093–34 108, 2015.
[41] V. Vasyl and S. Marat, "Correlation between topological structure and its properties in dynamic singular vector fields," *Appl. Opt.*, vol. 55, no. 12, pp. B28–B30, Apr. 2016.
[42] Ruchi, S. K. Pal, and P. Senthilkumaran, "Generation of V-point polarization singularity lattices," *Opt. Express*, vol. 25, no. 16, pp. 19 326–19 331, Aug. 2017.
[43] S. K. Pal and P. Senthilkumaran, "Lattice of C points at intensity nulls," *Opt. Lett.*, vol. 43, no. 6, pp. 1259–1262, 2018.
[44] X. Pang, J. Zhang, and X. Zhao, "Polarization dynamics on optical axis," *Opt. Commun.*, vol. 421, pp. 50–55, 2018.
[45] B. Richards and E. Wolf, "Electromagnetic diffraction in optical systems, II. Structure of the image field in aplanatic systems," *Proc. Roy. Soc. A*, vol. 253, pp. 358–379, 1959.
[46] M. Born and E. Wolf, *Principles of Optics: Electromagnetic Theory of Propagation, Interference and Diffraction of Light*, seventh (expanded) ed. Cambridge, U.K.: Cambridge Univ. Press, 1999.
[47] G. J. Gbur, *Mathematical Methods for Optical Physics and Engineering*. Cambridge, U.K.: Cambridge Univ. Press, 2011.